Characterization of electron beam induced modification of thermally grown SiO_2

J. R. Barnes, A. C. F. Hoole, M. P. Murrell, M. E. Welland, and A. N. Broers
Engineering Department, University of Cambridge, Trumpington Street, Cambridge CB2 1PZ, United Kingdom

J. P. Bourgoin,[a] H. Biebuyck,[b] M. B. Johnson,[c] and B. Michel
IBM Research Division, Zurich Research Laboratory, CH-8803, Rüschlikon, Switzerland

(Received 1 May 1995; accepted for publication 5 July 1995)

We used local probe techniques to characterize electron beam (e-beam) induced changes in thin oxides on silicon. Primary effects of the 1 nm wide, 300 keV e beam included the formation of positive charges trapped in the SiO_2, physical restructuring in the oxide, and deposition of carbonaceous compounds. Charges remained stable in thicker oxides (460 nm) and appeared as changes in the contact potential or microwave response with widths down to 100 nm. In thinner oxides (20 nm) the amount of charge was smaller and less stable; below 7 nm no charge was detected. Physical changes in the oxide, evident as a swelling of irradiated areas, accounted for the etching selectivity of these regions. © *1995 American Institute of Physics.*

Understanding the mechanisms of charge accumulation in an insulating SiO_2 layer using high-energy electron beams poses several scientific and technical challenges.[1–3] Charging occurs through a process of ionization by electron impact that renders initially neutral sites positive, the highest ionization probabilities occurring at defect structures in the oxide such as bridging vacancies.[3] The extent of the charged region for a focused incident electron beam depends on the thickness of the oxide and the dose and energy of the injected electrons, although charge does not accumulate at any depth unless the injected electrons have an energy of at least 7 eV, the activation energy for electron loss by electron impact. Typical saturation charge densities for SiO_2 are $\sim 10^{-5}$ e/nm[3]; variation in this density results primarily from the variability in defect density created in the oxide during growth. The Coulomb repulsion associated with induced fixed charge causes large mechanical stresses in irradiated regions. These stresses in turn may affect local oxide density and the chemical etch rate, an important consideration where e-beam exposure of Si/SiO_2 is used as part of a direct-write process.

This letter examines the interaction of high-energy (300 keV) electrons with Si/SiO_2. Atomic force microscopy (AFM) and scanning surface harmonic microscopy (SSHM) are used to characterize the physical and electronic consequences of high-energy electron beam irradiation. Using these techniques we focus on two effects: the modification of substrate properties such as density and dielectric constant; and the accumulation of charges trapped in the oxide film layer. Our techniques permit the study of these processes with high spatial resolution on the scale of the probe, which is typically in the nanometer range.

The electron beam lithography system used in this work was a JEOL JEM-4000 scanning transmission electron microscope (STEM). The addition of external computer control over the beam deflection and beam blanking add lithographic capabilities to the microscope over a range of energies from 75 to 400 keV. The focused spot size of the electron beam at 300 keV was ~ 1 nm.

Silicon substrates had a $\langle 100 \rangle$ orientation and n-type doping with resistivities between 8 and 12 Ωcm. The 20 and 460 thick oxide layers were grown thermally at $\sim$1000 °C in a humidified N_2 environment; the 7 nm thick oxide was grown in dry O_2. Each wafer was cleaned in 5:1:1 H_2O:H_2SO_4:HCl, followed by a final rinse with reagent grade isopropanol.[4,5] E-beam lithography at 300 keV defined an irradiated pattern of parallel lines, each line separated by 1 μm at doses ranging from 10 μC/m to 5 mC/m. The e-beam spot size was maintained at 1 nm. Substrates were heated to 200 °C during irradiation (see below).

We used three scanning probe techniques to characterize the samples: contact-AFM measured the topography, contact-potential AFM detected local changes in the contact potential (CP)[6,7] and SSHM[8] detected local changes in the high-frequency capacitance of each sample. In CP–AFM, an ac voltage modulation, at a frequency f, applied to the sample (typically 1–5 V peak to peak) produces signals $F_1 = 2V_m \phi G$ at f and $F_2 = \sqrt{2} V_m^2 G$ at $2f$, where V is the applied bias, ϕ is the CP difference between the tip and sample, and G is a function of the dielectric constant and thickness of the oxide, the tip–sample separation, and the tip radius.[9] Control of the AFM feedback loop using the $2f$ signal kept G constant so that the signal at f was independent of variations in G. The voltage required to null the signal at f provided a direct measure of the contact potential. The samples were stored under vacuum to minimize water and mobile ion contamination of the surface that might screen CP differences, although the measurements were made in air at a relative humidity of $\sim$50%, generally within 1–2 h after removal of the sample from vacuum.[10] Conducting tips had 30 nm of Al deposited directly onto silicon nitride cantilevers with force constants of $\sim$ 0.6 N m. SSHM is a scanning

[a]On leave from CEA/SCM CE Saclay, 91191, Gif/Yvette Cedex, France.
[b]Electronic mail: hbi@zurich.ibm.com
[c]Present address: Dept. of Physics and Astronomy, University of Oklahoma, Norman, OK 73072.

 0003-6951/95/67(11)/1538/3/$6.00

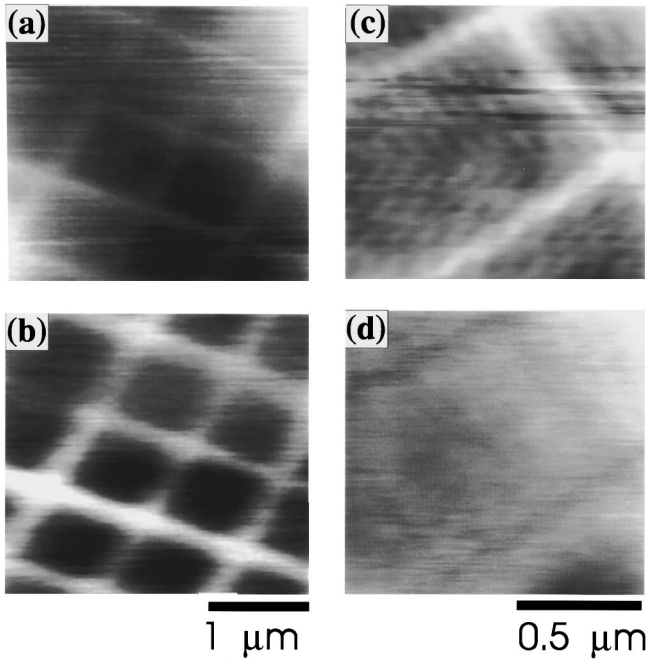

FIG. 1. CP–AFM image of e-beam patterned [(a) and (b)] 460 nm and [(c) and (d)] 20 nm SiO_2 on Si. The grid pattern is produced by e-beam irradiation with lines at an alternating dose of 1.6 and 5 mC/m. (a), (c) Constant second harmonic contour ($2f$) that follows topographical or capacitance changes on the samples, indicating either a local dielectric constant change, topographical change, or both, in irradiated areas. Contact AFM shows a swelling of the oxide in irradiated areas of ~10%. (b), (d) Response at the cantilever excitation frequency f (acquired simultaneously with the images at $2f$) that measures changes in the contact potential on the irradiated grid pattern.

tunneling microscope operating in a microwave cavity with a rf signal added to the dc bias; generation of the higher harmonics of this microwave signal occurring in the tip–substrate gap can be measured using standard 50 Ω microwave equipment.[8,11,12] All SSHM measurements here used etched tungsten tips with radii of curvature of ~30 nm. The samples were imaged in humidified air (R.H. ~75% at room temperature) and the tip potential was constant, typically −100 mV. The microwave signal applied to the substrate–tip junction was 1.6 V (peak to peak, 2 dBm) at 900 MHz. The third harmonic TH (2.7 GHz) of this signal, controlled the vertical height of the tip with respect to the surface.

One concern in this investigation was the accumulation of contamination on the surface of the oxide during e-beam irradiation that might affect subsequent measurements. Indeed, contact AFM confirmed changes in the topography of the surface after irradiation at room temperature in the moderate vacuum of the STEM chamber (10^{-7} mbar) caused by carbon contamination deposited during the writing process.[13] To overcome this effect all substrates were heated to 200 °C during irradiation to prevent detectable (by AFM) accumulation of contaminants.

Figures 1(a) and 1(b) show images acquired by CP–AFM at $2f$ and f, respectively, on a 460 nm oxide. A grid pattern that correlates with the lines of electron beam irradiation is evident in both images. In Fig. 1(a), this contrast is a consequence of changes in both the dielectric constant and topography as the oxide swells after irradiation.[14] The contrast in Fig. 1(b) results from trapped positive charges in the oxide that modify the local CP; the sign of these charges is measured directly from the sign of the applied nulling potential. The linewidth of accumulated positive charges is between 100 and 200 nm, much wider than the focus of the incident high-energy electron beam. This difference in width is mainly a consequence of the poor electronic screening in thick oxides that allows variations in the contact potential outside of the charged region due to fringing effects of the field. Figures 1(c) and 1(d) show images acquired by CP–AFM on a 20 nm oxide. The topographic image is similar to that in Fig. 1(a): the height of the features in irradiated areas showed that the oxide swelled by ~10% of its thickness. Figure 1(d) shows a reduction of the CP response in the 20 nm oxides and a reversal of contrast compared to that of the thicker oxide. This reversal of contrast results from either trapped negative charge or some physical change in the irradiated oxide resulting in a modified local CP. We favor the latter explanation because trapped charge appeared positive in thicker oxides and we observed a physical swelling of the oxide by contact AFM. Negative charges, trapped low energy secondaries for example, have a low barrier to detrapping (~1 eV) in the oxide and probably anneal out because of the high substrate temperature during irradiation. CP–AFM measured no change in the contact potential for thinner 7 nm oxide layers, although topographical contrast remained. The observation of no charge accumulation in thin (<10 nm) oxide is consistent with the results of others.[3] The detrapping of charge is driven by the potential difference at the Si/SiO_2 interface created by the charges trapped in the SiO_2 and may be enhanced by the ac bias voltage required to make the CP measurement, leading to the dissipation of charge in the 20 nm oxide.

SSHM overcame the detrapping problem in the 20 nm oxide, probably because of the higher frequency and lower amplitude field in SSHM, and thus allowed the detection of trapped positive charge in these samples. Figure 2(a) shows spatial changes in the TH signal on a 20 nm oxide exposed to a beam of 300 keV electrons at varying doses measured in the SSHM. The image is a map of the voltage applied to the Z piezo necessary to maintain a constant TH signal. The white lines in this figure correspond to regions that received electron irradiation. These lines were most evident for doses of electrons above 100 μC/m; we estimate a detection limit of 10 μC/m for newly prepared samples (<48 h old). The pattern at higher doses was stable for months. Figure 2(b) shows a grayscale top view of the TH response as a function of dc sample bias and position along the dotted line indicated in Fig. 2(a). The bright features result from peaks in the spectra recorded at intervals of 40 nm along the line. The TH versus dc bias spectrum of the surface not exposed to the electron beam [upper line in Fig. 2(b)] shows four peaks. The two large peaks reflect the voltage depletion of the majority carrier characteristic of the dopant type and concentration in the silicon sample.[11] These peaks are well modeled as the second derivative of the capacitance versus dc bias curve. The smaller peaks at negative voltage originate from minority carrier generation (the inversion region in the

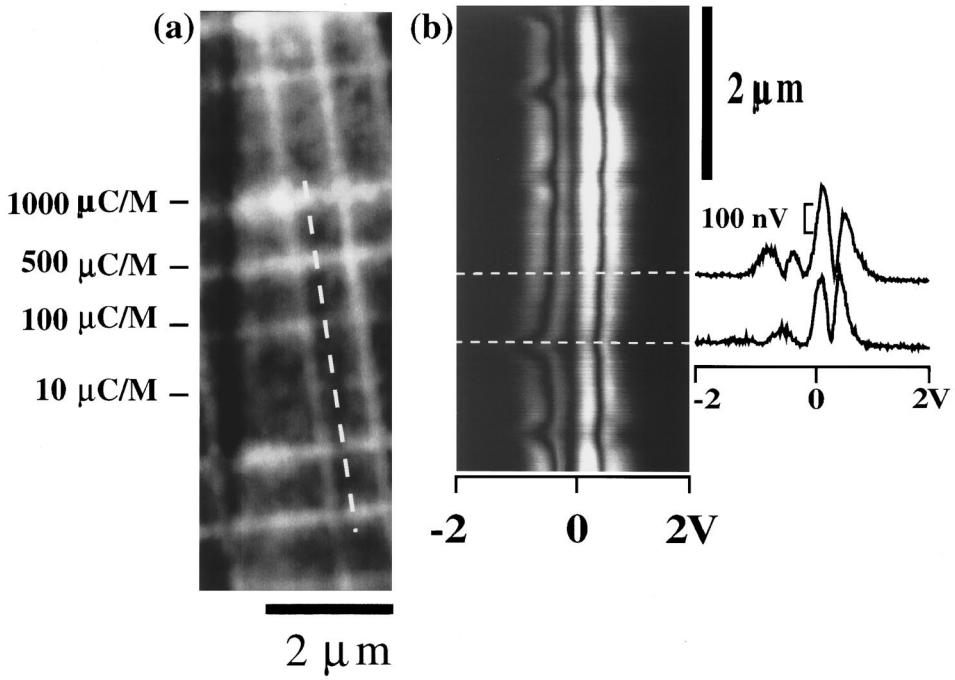

FIG. 2. (a) A constant TH image of an e-beam patterned SiO_2, 20 nm thick, on Si. The bright lines result from exposure to 1000, 500, 100, and 10 μC/m doses, respectively (the latter remained unresolved in the image). (b) Top view of TH vs dc bias and position along the dashed line in (a) shows variations in the TH response. The line profiles indicate the magnitude of TH in silica (top) and irradiated silica (bottom).

semiconductor).[11] These peaks are strongly affected by surface states and defects in the bulk material and are sensitive to illumination by visible light.[11] On the e-beam irradiated area the TH versus dc bias spectrum shifts to more negative values and the peaks are attenuated compared to those in unirradiated areas. The magnitude of the shift in the spectrum found in irradiated areas increased with the dose of 300 keV electrons, consistent with a higher level of positive charge in the semiconductor.

Our data show that the interaction of an e beam with SiO_2 results in physical restructuring and charge injection into the oxide. The overall effect of e-beam irradiation appeared as a swelling of the oxide concurrent with the creation of positively charged defect sites in the bulk. The charges dissipate from these traps in SiO_2 where the oxide layer is thinner than 7 nm. Pattern transfer to the silicon using a *p* etch (15:10:300 HF:HNO_3:H_2) showed that the area of the removed oxide was not much wider (10 nm) than the primary e beam, whereas electronic effects of charging measured by either CP–AFM or SSHM occurred over a much wider area (100 nm).[15] This observation suggests that selective etching of irradiated SiO_2 occurred because of the change in oxide density and not the effects of trapped charge.

J.B. and A.H. acknowledge funding from the ESPRIT project PRONANO (8523). H.B. and B.M. acknowledge partial funding by the BBW Schweiz within the ESPRIT basic research Project PRONANO (8523).

[1] E. H. Snow, A. S. Grove, and D. J. Fitzgerald, Proc. IEEE **55**, 1168 (1967).
[2] C. T. Sah, Solid State Electron. **33**, 147 (1990).
[3] S. E. Thompson and T. Nishida, J. Appl. Phys. **72**, 4683 (1992).
[4] D. B. Fenner, D. K. Biegelsen, and R. D. Bringans, J. Appl. Phys. **66**, 419 (1989).
[5] Y. Nakagawa, A. Ishitani, T. Takahagi, H. Kuroda, H. Tokumoto, M. Ono, and K. Kajimura, J. Vac. Sci. Technol. B **8**, 262 (1990).
[6] B. D. Terris, J. E. Stern, D. Rugar, and H. J. Mamin, Phys. Rev. Lett. **63**, 2669 (1989).
[7] B. D. Terris, J. E. Stern, D. Rugar, and H. J. Mamin, J. Vac. Sci. Technol. A **8**, 374 (1990).
[8] B. Michel, W. Mizutani, R. Schierle, A. Jarosch, W. Knop, H. Benedickter, W. Bachtold, and H. Rohrer, Rev. Sci. Instrum. **63**, 4080 (1992).
[9] C Schönenberger and S. F. Alvarado, Phys. Rev. Lett. **65**, 3162 (1990).
[10] M. Nonnenmacher, M. P. O'Boyle, and H. K. Wickramasinghe, Appl. Phys. Lett. **58**, 2921 (1991).
[11] J.-P. Bourgoin, M. B. Johnson, and B. Michel, Appl. Phys. Lett. **65**, 2045 (1994).
[12] M. B. Johnson, J.-P. Bourgoin, and B. Michel, Micro Nano Eng. **27**, 539 (1995).
[13] J. R. Barnes, A. C. F. Hoole, M. P. Murrell, M. E. Welland, and A. N. Broers (unpublished).
[14] P. E. Allen, D. P. Griffis, Z. J. Radzimski, and P. E. Russell, J. Vac. Sci. Technol. A **10**, 965 (1992).
[15] A. C. F. Hoole and A. N. Broers, J. Vac. Sci. Technol. B **10**, 2855 (1992).